# Proton Transfer Impedance of Electrodes Modified with Acid Thiol Monolayers

*Antonio M. Luque,*[a] *Willem H. Mulder,*[b] *Juan José Calvente* [a] *and Rafael Andreu* [a,*]

[a] Departamento de Química Física. Universidad de Sevilla. 41012-Sevilla, Spain

[b] Department of Chemistry, The University of the West Indies, Mona Campus, Kingston 7, Jamaica.

[*] Corresponding author: Phone: +34-954557177, Fax: +34-954557174

E-mail: fondacab@us.es

## Abstract

Analytical expressions describing the electrochemical impedance spectrum of a metallic electrode modified with an acid thiol monolayer, that undergoes a potential-induced proton transfer, have been derived from an electrostatic model of the interface. The frequency dispersion of the electrode impedance is described by an equivalent circuit that bears some similarities with that associated with a surface redox process. Good agreement is found between the theoretical predictions and the impedance of a Au(111) electrode modified with a 11-mercaptoundecanoic monolayer recorded as a function of ac frequency, dc potential and surface concentration of electrochemically active carboxylic groups. The same thermodynamic and kinetic parameter values are obtained from independent analysis of the voltammetric and impedimetric responses, except in the case of the reorganization energy for proton transfer, which seems to be affected by a slow potential-induced reorientation and dissociation of the external acid groups of the monolayer.



**Keywords:** Self-assembled monolayers, 11-mercaptoundecanoic acid, potential-induced dissociation, electrode impedance, proton transfer.

## 1. Introduction

The electrode potential provides a convenient tool to control the thermodynamics and kinetics of typical electrochemical processes, such as electron transfer [1] or cation deposition [2]. Moreover, other processes involving adsorbed species, such as dissociation of weak acids, can also be manipulated through the electrode potential. In fact, *in situ* spectroscopic measurements have shown an increase of the dissociation degree of adsorbed acids as the potential is made more positive [3,4], a behavior that is consistent with Wien's secondary effect. These types of non-faradaic processes can become amenable to study by conventional electrochemical techniques, inasmuch as the resulting charge displacement can eventually be observed as a current flow under potentiostatic conditions [5].

Molecular self-assembly of thiol monolayers is commonly used to modify metallic substrates in a predetermined way [6-8]. By an adequate choice of the monolayer composition, reactive functionalities can be immobilized in the vicinity of the electrode surface. Thus, White et al. [9] were the first to report the electrochemical characteristics associated with a potential-induced protonation / deprotonation of an acid thiol monolayer. They analyzed the voltammetric response of a Ag(111) electrode coated with a mixed monolayer of 11-mercaptoundecanoic acid (MUA) and 1-decanethiol, and showed that it was similar to that of a surface-confined redox probe, but including also some specific variations of peak area and potential with the solution pH. The same behavior was observed later with gold electrodes modified with monolayers of MUA [10-12], 4-mercaptobenzoic acid [13], 3-mercaptopropylphosphonic acid [14] and 2-dimethylaminoethanethiol [15], and

is consistent with an increase in the degree of acid dissociation as the potential is made more positive. However, the opposite trend (i.e. a decrease in the degree of dissociation at more positive potentials) has also been observed in quartz microbalance [16] and infrared absorption [17-19] experiments performed on gold electrodes modified with ω-mercaptoalkanoic monolayers, and has been explained in terms of a cation-exchange mechanism, to the effect that the strength of electrostatic adsorption of cations in the diffuse layer favors their exchange with the protons of the immobilized carboxylic groups at negative potentials.

Recently, we have developed an electrostatic model [11,12] that accounts for these observations in terms of two populations of carboxylic groups. In our model, the large majority of carboxylic groups are in contact with the electrolyte solution and far from the electrode surface. Dissociation of this population is only weakly affected by changes in the electrode potential, but can still be modified indirectly by the potential-induced adsorption / desorption of nearby cations. The second population consists of a small number of carboxylic groups that are buried inside the organic layer, close to the electrode surface, and presumably held there by image forces [12]. Their dissociation is strongly influenced by the electrode potential, and only weakly affected by the adsorption of cations in the outer part of the monolayer. The model predicts that the potential-induced protonation / deprotonation of the latter population should produce non-faradaic voltammograms similar to those of a surface-confined redox probe [20], in agreement with experimental findings [9-15]. Though the model does not speculate on this population's physical origin, it is likely that it consists of physisorbed mercaptoalkanoic molecules, since their surface

concentration increases with the thiol concentration in the deposition solution and the time the electrode is immersed in it 12].

Besides displaying opposite responses to changes in the applied potential, the two populations of carboxylic groups also differ in the time scale of those responses. A comparison of the evolution of surface infrared spectra of MUA monolayers with time [19], collected under low potential-scan rate conditions, and their voltammetric response [11] suggests that the ion exchange mechanism is much slower than the direct proton transfer mechanism. In order to contend with two processes that operate on different time scales, it would be desirable to carry out a detailed analysis of the impedance of these electrodes as a function of the ac perturbation frequency [21]. The first attempt was due to Burgess et al. [10], who described the frequency dependence of the charge rearrangement associated with a potential-induced protonation process as a series connection of a resistance $\left(R_{p/dp}\right)$ and a capacitance $\left(C_{p/dp}\right)$. Then, the electrode impedance was intuitively derived as a parallel connection of this protonation impedance and the monolayer capacitance. This equivalent circuit was shown to fit satisfactorily the frequency dependence of the electrode impedance, but the number of parameters and the empirical approach of their derivation precluded a satisfactory interpretation of the elements of their equivalent circuit.

In the present work, we derive an explicit analytical expression for the impedance of an electrode modified with an acid thiol monolayer, on the basis of an electrostatic description of the electrode and of our previous model for a potential-induced proton transfer process, that assumes the adequacy of a nonadiabatic mechanism. We have also measured the impedance of a MUA-modified Au(111) electrode as a function of the ac frequency, dc potential and surface concentration of embedded carboxylic groups, and have

found a quantitative agreement between the theoretical predictions and the experimental results.

## 2. Material and methods

11-Mercaptoundecanoic acid (MUA) was purchased from Aldrich. High purity Puratronic sodium fluoride was from Alfa Aesar. Water was purified with a Millipore Milli-Q system (resistivity 18 MΩ cm). The solution pH was adjusted to 8.5 in the electrochemical cell by adding a few drops of a freshly prepared ~1 mM NaOH (Fluka) solution to a previously de-aerated 20 mM NaF solution. The pH was continuously monitored with an Orion 8102BN electrode connected to an Orion 420A pH meter.

A Au(111) single crystal electrode (Metal Crystals and Oxides), with a geometric basal surface area of 0.225 $cm^2$, was used as working electrode. Self-assembled monolayers (SAMs) of MUA with 3.5, 10 and 20 pmol $cm^{-2}$ of embedded carboxylic groups were obtained by immersing the Au(111) surface in a 50 mM MUA ethanolic solution for 1, 2.5 and 3 h, respectively, while those with 40 pmol $cm^{-2}$ were obtained by contacting the gold surface with a 18 mM MUA ethanolic solution for 19 h. The modified electrode was first rinsed with ethanol and then with a 5 mM NaF aqueous solution at pH 8.5. Contact of the thiol-coated Au(111) surface with the electrolyte solution in the electrochemical cell was made by the hanging meniscus configuration, and it was allowed to equilibrate with the solution for 5 min. prior to performing the electrochemical measurements. A Ag|AgCl|NaCl (sat'd) electrode and a Pt wire were used as reference and auxiliary electrodes, respectively. The reference electrode made electrical contact with the cell solution via a salt bridge filled with the same cell solution. All measurements were

performed in a water-jacketed glass cell, thermostated at 25.0 ± 0.2ºC with a Haake D8.G circulator thermostat. Electrolyte solutions were de-aerated with a presaturated argon stream prior to the measurements, and a positive argon pressure was maintained over the solution during the measurements. All the potential values are referred to the Ag|AgCl|NaCl (sat'd) electrode. Voltammetric and cell impedance measurements were carried out with an Autolab PGSTAT30 (Eco Chemie). After applying the required dc potential, a 3 s delay was observed to allow for monolayer stabilization. Subsequently, a 5 mV rms sinusoidal perturbation was applied and impedances were recorded at 20 frequencies in the 0.5 $s^{-1} \leq f \leq 5000\ s^{-1}$ range.

## 3. Theory

We have shown previously [11,12] that the voltammetric response of mercaptoalkanoic monolayers can be described quantitatively by assuming that the thiol monolayer contains two populations of carboxylic groups. The first consists of those carboxylic groups that are exposed to the external solution, and whose degree of ionization varies very slowly with the applied potential, so that it can be assumed that it is determined only by the interaction with the contents of the solution. The second includes those carboxylic groups that are buried inside the monolayer, and whose degree of ionization is controlled not only by the solution pH but also by the electrode potential. We denote by $\Gamma_T^{ext}$ and $\Gamma_T^{p/dp}$ the surface concentrations of the external and buried carboxylic groups, respectively. The buried carboxylic (R-OH) and carboxylate ($R\text{-}O^-$) groups are assumed to be located at a plane *a* (see Figure 1), parallel to the electrode surface. The proton exchange also involves a proton acceptor ($OH^-$) and a proton donor ($H_2O$) from solution, which share

a common plane (*b*) of closest approach to the electrode surface (see Figure 1). Other electrolyte ions are allowed to approach the electrode up to plane *d* only, which can be identified with the Outer Helmholtz Plane. The average potential values at the first two planes, $\phi^a$ and $\phi^b$, with respect to the bulk solution ($\phi^s = 0$) can be expressed in terms of the electrode potential $\phi^m$, as follows:

$$\phi^a = \phi^d + \omega_a \left( \phi^m - \phi^d - \frac{\theta_{R-O^-} F \Gamma_T^{p/dp}}{K_{ma}} \right) \tag{1}$$

where $\phi^d$ is the potential drop across the diffuse layer, $\theta_{R-O^-}$ is the degree of ionization of buried carboxylic groups, $\omega_a = K_{md} / K_{ad}$ is the ratio of the integral capacity of the solvated monolayer ($K_{md}$) and that of the dielectric slab bounded by plane *a* and the diffuse layer boundary *d* ($K_{ad}$), so that $0 < \omega_a < 1$, and $K_{ma}^{-1} = K_{md}^{-1} - K_{ad}^{-1}$.

Analogously,

$$\phi^b = \phi^d + \omega_b \left( \phi^m - \phi^d - \frac{\theta_{R-O^-} F \Gamma_T^{p/dp}}{K_{ma}} \right) \tag{2}$$

where $\omega_b = K_{md} / K_{bd}$.

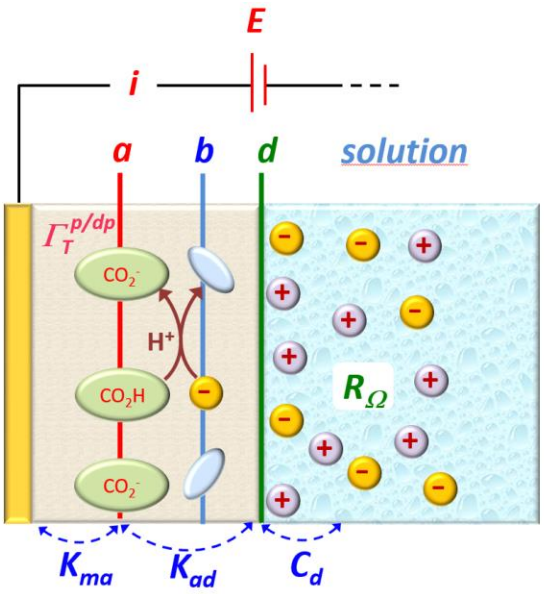


**Figure 1.** Schematic representation of the potential-induced proton transfer process at an electrode modified with a $\omega$-mercaptoalkanoic acid monolayer, which is in contact with an aqueous electrolyte solution. Carboxylate and carboxylic groups that are involved in the potential-induced proton transfer are located at plane *a* inside the monolayer. Proton donors and acceptors from solution are located at plane *b*. Other symbols are defined in the text.

---

On the basis of eqs. 1 and 2, quantitative relationships between the electrode potential $\phi^m$ and the extent of ionization $\theta_{R-O^-}$ can be derived under equilibrium and non-equilibrium conditions (see eqs. S5 and S7 in the Supporting Information section).

**a) Transient response of the modified electrode.** As stated before, a change in the electrode potential can trigger a proton exchange between monolayer and solution, producing a flow of non-faradaic current through the external circuit. Potential perturbation and current flow are related through the model parameters, and this relationship defines the transient response of the modified electrode.

The non-faradaic current density $i$ stems from a change in the charge density at the electrode surface $q^m$, which satisfies the electroneutrality condition at the interface:

$$q^m = -q^d + F\,\Gamma_T^{p/dp}\,\theta_{R-O^-} + F\Gamma_{R-O^-}^{ext} \tag{3}$$

where $q^d$ is the charge density in the diffuse layer and $\Gamma_{O-R^-}^{ext}$ is the surface concentration of ionized carboxylic groups in the external part of the monolayer. Therefore,

$$i = \frac{dq^m}{dt} = C_d \frac{d\phi^d}{dt} + F\Gamma_T^{p/dp} \frac{d\theta_{R-O^-}}{dt} \tag{4}$$

since $\Gamma_{R-O^-}^{ext}$ is assumed to depend on the solution pH only, and where $C_d$ is the diffuse layer capacity. Furthermore, the interfacial potential drop $\phi^m$ can be split into three contributions

$$\phi^m = \frac{q^m}{K_{md}} - \frac{F\Gamma_T^{p/dp}\theta_{R-O^-}}{K_{ad}} + \phi^d \tag{5}$$

which relate $q^m$ and $\phi^d$ at a given $\phi^m$. By taking the first derivative with respect to time, the following expression is obtained

$$\frac{d\phi^m}{dt} = \frac{i}{K_{md}} - \frac{F\Gamma_T^{p/dp}}{K_{ad}} \frac{d\theta_{R-O^-}}{dt} + \frac{d\phi^d}{dt} \tag{6}$$

The protonation / deprotonation rate in the second term of the r. h. s. can be expressed as [11]:

$$\frac{d\theta_{R-O^-}}{dt} = k_{dp} c_{OH^-}^{sol} \left(1 - \theta_{R-O^-}\right) - k_p \theta_{R-O^-} \tag{7}$$

where $k_p$ and $k_{dp}$ are the protonation and deprotonation rate constants, respectively, and $c_{OH^-}^{sol}$ is the bulk concentration of the proton acceptor $OH^-$. By combining eqs. 4, 6 and 7, we obtain:

$$\frac{d\phi^d}{dt} = \frac{\dfrac{d\phi^m}{dt} + \dfrac{F\Gamma_T^{p/dp}\left(k_p\theta_{R-O^-} - k_{dp}c_{OH^-}^{sol}(1-\theta_{R-O^-})\right)}{K_{ma}}}{1+\dfrac{C_d}{K_{md}}} \tag{8}$$

The transient response of the modified electrode can now be obtained by solving numerically eqs. 7 and 8, after substituting for $C_d\left(\phi^d\right)$, $k_p$ and $k_{dp}$ as a function of the dependent variables $\theta_{R-O^-}$ and $\phi^d$ and the control variable $\phi^m(t)$.

**b) Impedance spectrum of the modified electrode.** To obtain an expression for the admittance $Z_{el}^{-1}$ of the modified electrode, we consider that the electrode, under equilibrium conditions at a potential $\phi^m$, is subjected to a small periodic perturbation of the potential $\Delta\phi^m \cdot e^{j\omega t}$, and that the current response is of the form $\Delta i \cdot e^{j\omega t}$, where $\omega$ is the angular frequency of the perturbation, $\Delta\phi^m$ and $\Delta i$ are the amplitudes of the perturbation and response, respectively, and $j=\sqrt{-1}$, so that $Z_{el}^{-1} = \Delta i / \Delta\phi^m$. Then, eq. 4 can be rewritten as:

$$\Delta i \cdot e^{j\omega t} = j\omega \cdot \left( C_d \frac{\Delta\phi^d}{\Delta\phi^m} + F\Gamma_T^{p/dp}\frac{\Delta\theta_{R-O^-}}{\Delta\phi^m}\right)\cdot \Delta\phi^m \cdot e^{j\omega t} \tag{9}$$

and,

$$Z_{el}^{-1}(j\omega) = \frac{\Delta i}{\Delta\phi^m} = j\omega \cdot \left( C_d \frac{\Delta\phi^d}{\Delta\phi^m} + F\Gamma_T^{p/dp}\frac{\Delta\theta_{R-O^-}}{\Delta\phi^m}\right) \tag{10}$$

The relationships between the $\Delta\theta_{R-O^-}$, $\Delta\phi^d$ and $\Delta\phi^m$ amplitudes can be derived from eqs. 6 and 8. After substituting for $\Delta\theta_{R-O^-}$ and $\Delta\phi^d$ into eq. 10 we obtain the frequency dispersion of the electrode admittance in terms of the model parameters (see the

Supporting Information section for a detailed derivation), which is shown to be identical to that of the equivalent circuit depicted in Figure 2a.

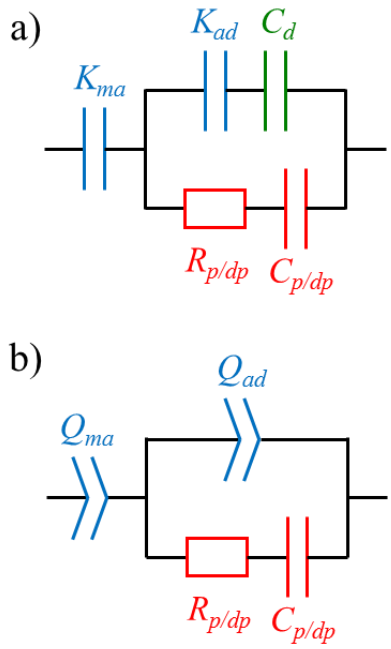


**Figure 2.** a) Theoretical equivalent circuit that describes the impedance of an electrode that undergoes a potential-induced protonation / deprotonation process. Circuit elements are defined in the text. b) Equivalent circuit of the electrode impedance, where the $K_{ma}$ and $K_{ad}$ capacitors have been replaced by the constant phase elements $Q_{ma}$ and $Q_{ad}$, respectively, and where the diffuse layer capacity $C_d$ has been neglected.

Besides the three capacitors $K_{ma}$, $K_{ad}$ and $C_d$, which have already been defined, the equivalent circuit in Figure 2a includes a series connection of the $R_{p/dp}$ resistance and the $C_{p/dp}$ capacitance. These last two elements contain the relevant information on the proton transfer process. General expressions of $R_{p/dp}$ and $C_{p/dp}$ are presented in the Supporting Information (eqs. S24 and S25) but they can be simplified under the usual experimental

conditions. Thus, we have shown [12] that whenever $\Gamma_{R-O^-}^{ext} \geq 100$ pmol cm$^{-2}$ the value of $\phi^d$ remains constant within the potential interval where proton exchange takes place. Then, $\phi^m - \phi_{1/2}^m = E - E_{1/2}$ where $E$ is the electrode potential measured with respect to the reference electrode and $E_{1/2}$ is its value when $\theta_{R-O^-} = \theta_{R-OH} = 0.5$ under equilibrium conditions, so that $C_{p/dp}$ and $R_{p/dp}$ can be expressed as:

$$C_{p/dp} = \frac{F^2 \Gamma_T^{p/dp}}{RT} \frac{\exp(\omega_a \varphi)}{\left(1+\exp(\omega_a \varphi)\right)^2} \tag{11}$$

$$R_{p/dp} = \frac{RT}{F^2 \Gamma_T^{p/dp}} \left( \frac{1}{k_p} + \frac{1}{k_{dp} c_{OH^-}^{sol}} \right) \tag{12}$$

where

$$\varphi = \frac{F}{RT} \left( E - E_{1/2} - \frac{\left(\theta_{R-O^-} - 1/2\right) F \Gamma_T^{p/dp}}{K_{ma}} \right) \tag{13}$$

The two rate constants $k_p$ and $k_{dp}$ vary with the applied potential according to [11]:

$$\ln k_p = \ln k_s^{ap} - \alpha_p^{ap} \varphi - \alpha_M \varphi^2 \tag{14}$$

$$\ln\left(k_{dp} c_{OH^-}^{sol}\right) = \ln k_s^{ap} + \alpha_{dp}^{ap} \varphi - \alpha_M \varphi^2 \tag{15}$$

where the parameters $\alpha_p^{ap}$, $\alpha_{dp}^{ap}$ and $\alpha_M$ are defined in eqs. S11-S13, and $k_s^{ap}$ is the apparent standard proton transfer rate constant, such that $k_s^{ap} = k_{dp} c_{OH^-}^{sol} = k_p$ when $E = E_{1/2}$.

The equivalent circuit in Figure 2a displays a frequency dispersion similar to that of the equivalent circuit derived by Burgess et al. [10] when $\omega_a \approx 1$, since then $K_{ma} >> K_{ad} \approx K_{md}$. Moreover, the expressions for $C_{p/dp}$ and $R_{p/dp}$ in terms of $k_p$ and $k_{dp}$ become identical in both derivations (i.e. eqs (11) and (12) above and eqs. (30) and (29) in

ref. [10], respectively) if it is assumed that all the carboxylic groups are involved in the proton transfer process (i. e. $\Gamma_T^{p/dp} = \Gamma_{tot} \approx 8 \cdot 10^{-10}$ mol/cm$^2$ ) and that Burgess' parameter $\lambda = \left( \partial\, q^m / \partial\, \theta_{R-O^-} \right)_E$ equates to $F \Gamma_T^{p/dp}$ . However, these authors could not provide a complete description of the proton transfer process due to the absence of an adequate procedure to analyze the equilibrium limit at each potential, and to extract the individual values of the protonation / deprotonation rate constants.

## 4. Results and discussion

### 4.1 Frequency and potential dependence of the cell impedance

The cell impedance ( $Z_{cell}$ ) consists of a series connection of the modified electrode impedance ( $Z_{el}$ ) and the ohmic resistance ( $R_\Omega$ ) originated mainly in the electrolyte solution, so that:

$$Z_{cell} = Z'_{cell} + j\, Z''_{cell} = R_\Omega + Z_{el} \tag{16}$$

where $Z'_{cell}$ and $Z''_{cell}$ are the real and imaginary components of the cell impedance, respectively, which can be related to the components of the equivalent circuit in Figure 2a according to:

$$Z'_{cell}(\omega) = R_\Omega + \frac{R_{p/dp}}{\left(1 + \frac{C_{as}}{C_{p/dp}}\right)^2 + \left(\omega R_{p/dp} C_{as}\right)^2} \tag{17}$$

$$-Z''_{cell}(\omega) = \frac{1}{\omega K_{ma}} + \frac{\frac{\left(1 + C_{p/dp}^{-1} C_{as}\right)}{\omega C_{p/dp}} + \omega C_{as} R_{p/dp}^2}{\left(1 + \frac{C_{as}}{C_{p/dp}}\right)^2 + \left(\omega R_{p/dp} C_{as}\right)^2} \tag{18}$$

where $C_{as}^{-1} = K_{ad}^{-1} + C_d^{-1}$ . Eqs. 17 and 18 show explicitly the dependence of the cell impedance on the ac perturbation frequency, and reveal some close similarities with those corresponding to a surface redox process [22,23]. However, the dependence on the applied potential $E$ remains implicit in these equations, since it arises from that of each equivalent circuit element. To visualize the variation of the cell impedance with frequency we have used Bode plots, in which the phase angle ( $\Phi$ ) and the logarithm of the impedance modulus ($|Z_{cell}|$), defined as:

$$\Phi = \arctan \frac{Z''_{cell}}{Z'_{cell}} \tag{19}$$

and

$$|Z_{cell}| = \sqrt{(Z'_{cell})^2 + (Z''_{cell})^2} \tag{20}$$

are plotted as a function of the logarithm of the ac frequency $f = \omega / 2\pi$ .

In the absence of a proton transfer process, $C_{p/dp} = 0$ and $R_{p/dp} = \infty$ , so that the protonation branch in the equivalent circuit is cancelled, and pure R-C behavior is predicted (see the red lines in Figures 3a and b). Then, the cell impedance is dominated by the ohmic resistance at high frequencies (so that $\Phi \approx 0^{\circ}$ and $|Z_{cell}| \approx R_{\Omega}$ ) and by the series connection of the $K_{ma}$ , $K_{ad}$ and $C_d$ capacitances at low frequencies (so that $\Phi \approx$ -90º and $\log|Z_{cell}| \propto \log f$ ).

The presence of the proton transfer process leads to the emergence of a minimum in the phase angle plot (see Figures 3a and 3c) and an inflection point in the impedance modulus plot (see Figures 3b and 3d). The minimum and the inflection point appear at the same characteristic frequency $f^*$ , which helps to locate an adequate frequency range to

carry out the experiments and it also provides an initial estimate of the rate of proton transfer, since $f^* \approx k_s^{ap}$. It may be observed also in Figure 3 how the extent of the deviation from the R-C limiting behavior is a measure of the surface concentration of acid groups $\Gamma_T^{p/dp}$ that are involved in the proton transfer process.

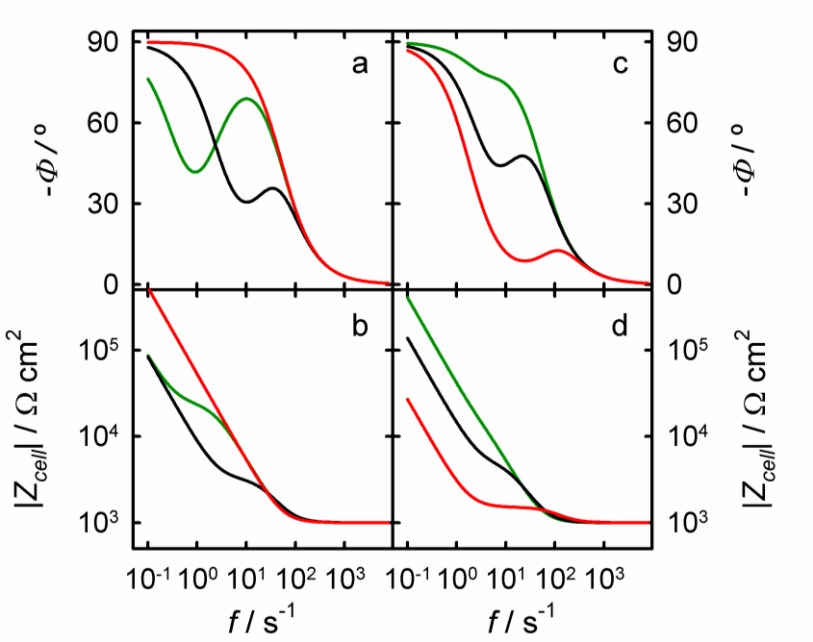


**Figure 3.** a) and b) Influence of $k_s^{ap}$ on the cell impedance, $k_s^{ap}$ / $s^{-1}$: 0 (red line), 1 (green line), 10 (black line). c) and d) Influence of $\Gamma_T^{p/dp}$ on the cell impedance, $\Gamma_T^{p/dp}$ / pmol $cm^{-2}$: 1 (green line), 10 (black line), 100 (red line). Default parameter values: $\Gamma_T^{p/dp}$ = 20 pmol $cm^{-2}$, $k_s^{ap}$ = 10 $s^{-1}$, $\omega_a = 0.98$, $R_\Omega = 1000\ \Omega\ cm^2$, $K_{md} = 3\ \mu F\ cm^{-2}$, $T$ = 298 K. Cell impedances have been computed assuming that $E = E_{1/2}$ and $C_d >> K_{ad}$.

In the case of MUA monolayers in contact with dilute basic solutions it can safely be assumed [11,12] that $C_d >> K_{ad}$ and that both $\omega_a$ and $K_{md}$ are independent of the applied potential. Therefore, any variation of the cell impedance with the dc potential will

originate in those of $C_{p/dp}$ and $R_{p/dp}$, which depend on the values taken by $k_p$, $k_{dp}$ and $\theta_{R-O^-}$ at each potential, according to eqs. 11-13. A closer look at these equations reveals that the proton transfer capacitance $C_{p/dp}$ is related to parameters describing the proton transfer equilibrium, whereas the relevant kinetic parameters are all included in the proton transfer resistance $R_{p/dp}$.

Since $C_{p/dp} \propto \theta_{R-O^-}\left(1-\theta_{R-O^-}\right)$ at each potential (see eq. S24), $C_{p/dp}$ is a scaled version of the dc voltammetric current under equilibrium conditions [20,24], and we can expect a bell shaped dependence of $C_{p/dp}$ with the applied potential, with a maximum at $E_{1/2}$ (see Figures 4b and 4d). Analogously, $R_{p/dp} \propto k_p^{-1} + \left(k_{dp} c_{OH^-}^{sol}\right)^{-1}$ and the variation of $R_{p/dp}$ with the applied potential will reproduce those of $k_p$ and $k_{dp}$, which are determined by the values of the parameters $\alpha_p^{ap}$, $\alpha_{dp}^{ap}$ and $\alpha_M$, according to eqs. 14 and 15. In the simplest case, when $\alpha_p^{ap} = \alpha_{dp}^{ap}$ and $\alpha_M = 0$, the $R_{p/dp}$ vs. $E$ plots take the form of a hyperbolic cosine with a minimum at $E_{1/2}$ (Figures 4a and 4c). More general cases for $\alpha_p^{ap} / \alpha_{dp}^{ap} \neq 1$ and $\alpha_M \neq 0$ are considered in the Supporting Information section. Figure 4 also shows the influence of the number ($\Gamma_T^{p/dp}$) and location ($\omega_a$) of the buried carboxylic groups on the potential dependence of $C_{p/dp}$ and $R_{p/dp}$. It may be observed that $\Gamma_T^{p/dp}$ acts simply as a scaling factor, without modifying the aforementioned basic shapes. However, a decrease of $\omega_a$ results in a broadening of the $C_{p/dp}$ and $R_{p/dp}$ vs. $E$ plots, since it makes the potential at the protonation / deprotonation site $\phi^a$ less sensitive to changes in the electrode potential $\phi^m$.

It may be concluded from Figure 4 that proton transfer impedances are more conveniently obtained at potentials close to $E_{1/2}$. As $E$ moves away from $E_{1/2}$, both $R_{p/dp}$ and $1/C_{p/dp}$ increase, and eventually $Z_{p/dp} >> 1/\ j\omega C_{as}$, so that:

$$\left(Z_{cell}\right)_{\left|\phi^m-\phi^m_{1/2}\right|\to\infty} \approx R_\Omega + \frac{1}{j\omega}\left(\frac{1}{K_{ma}}+\frac{1}{C_{as}}\right) \approx R_\Omega + \frac{1}{j\omega K_{md}} \tag{21}$$

and any information on the proton transfer process is lost.

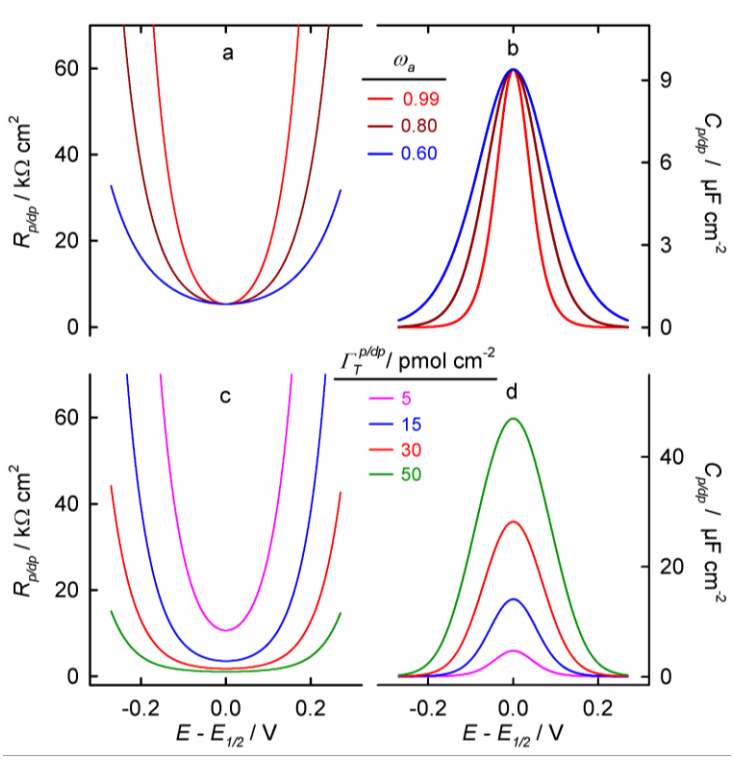


**Figure 4.** a) and b) Influence of $\omega_a$ on the variation of $R_{p/dp}$ and $C_{p/dp}$ with the applied potential. c) and d) Influence of $\Gamma_T^{p/dp}$ on the variation of $R_{p/dp}$ and $C_{p/dp}$ with the applied potential. Default parameter values: $\Gamma_T^{p/dp}$ = 10 pmol cm$^{-2}$, $k_s^{ap}$ = 10 s$^{-1}$, $\omega_a = 0.9$, $\alpha_p^{ap} = \omega_a / 2$, $\alpha_M = 0$, $K_{md} = 3\ \mu$F cm$^{-2}$, $\Gamma_{R-O^-}^{ext}$ = 400 pmol cm$^{-2}$, $T$ = 298 K.

### 4.2 Comparison with experiment

Rather than attempting a direct fit of the cell impedances to the equivalent circuit depicted in Figure 2a, we will analyze first the impedance spectrum at potentials well away from $E_{1/2}$, where eq. 21 holds. In a previous voltammetric study of the same electrode we obtained $\left(E_{1/2}\right)_{\Gamma_T^{p/dp}\to 0} = -0.23\ \mathrm{V}$, so that no potential-induced proton transfer is expected to take place for $E \le -0.35\ \mathrm{V}$ (where $\theta_{O-R^-} \approx 0$) and for $E \ge -0.11\ \mathrm{V}$ (where $\theta_{O-R^-} \approx 1$). It may be observed in Figure 5 how cell impedances take the same values at potentials close to the indicated positive and negative limits. It is also evident that eq. 21 can only reproduce satisfactorily the experimental Bode plots at high frequencies, i.e. for $f > 100\ \mathrm{s}^{-1}$ (dashed lines). At low frequencies, $\left|Z_{cell}\right|$ deviates moderately from the behavior predicted by eq. 21, but a more pronounced deviation is observed for the phase angle, which reaches a low frequency plateau at ~ -80º rather than the expected -90º. Similar results have been obtained for other hydrophilic SAMs, and have been ascribed to a slow ion/water penetration into the SAM [25]. It should be noted that Burgess et al. [10] reported a low-frequency phase angle plateau of ~ -88º for their MUA monolayers deposited on polycrystalline gold beads, which suggests that their monolayers were less permeable than ours.

To account for the measured low-frequency phase angle values, the interfacial capacitance $K_{md}$ was replaced by a constant phase element (CPE) $Q_{md}$, whose impedance takes the form $\left(Z_{CPE}\right)_{md} = 1/\left(Q_{md}\cdot\left(j\omega\right)^{n_\alpha}\right)$, with $0 < n_\alpha < 1$ [10]. In these electrodes, the CPE is likely to originate in a slow spatial redistribution of charges and dipoles (such as water molecules or polar groups tethered to the monolayer) in response to the externally

imposed ac perturbation [26-28]. Such redistribution can certainly include the slow potential-induced protonation / deprotonation of the external carboxylic groups via an ion-exchange mechanism [17-19]. A satisfactory fit of the observed impedance spectrum at potentials far from $E_{1/2}$ was obtained when the capacitive term in eq. 21 was replaced by a CPE with $Q_{md} = 4.2 \cdot 10^{-6}\ \Omega^{-1}\ s^{n_\alpha}\ cm^{-2}$ and $n_\alpha = 0.91$ (solid lines in Figure 5).

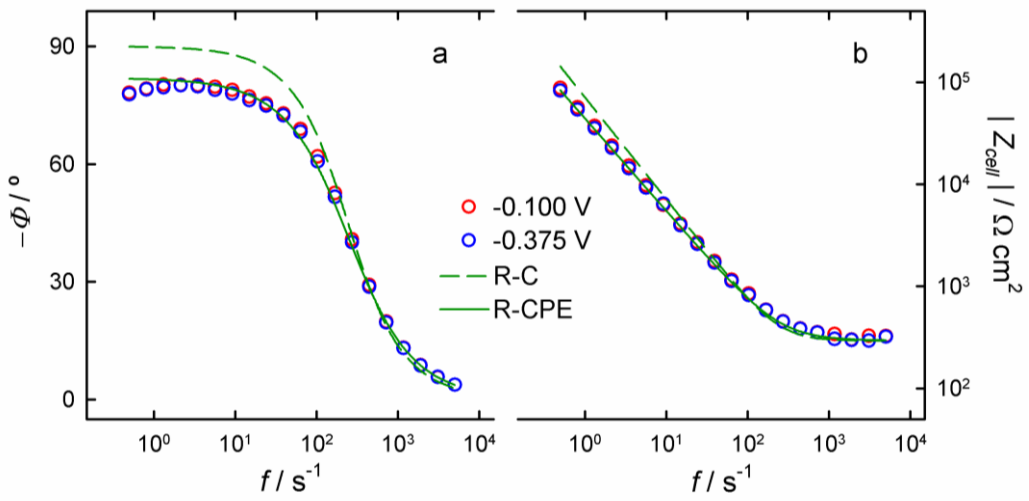


**Figure 5.** a) Phase angle and b) impedance modulus Bode plots of a Au(111) electrode modified with a MUA monolayer, contacting a 20 mM NaF aqueous solution of pH 8.5 at 298 K. Impedances were measured at -0.100 V (○) and -0.375 V (○). Dashed lines (— —) have been computed from eq. 21 with $R_\Omega = 290\ \Omega\ cm^2$ and $K_{md} = 2.2\ \mu F\ cm^{-2}$. Continuous lines (——) have been computed from a series connection of $R_\Omega = 290\ \Omega\ cm^2$ and a constant phase element (CPE) $Q_{md} = 4.2 \cdot 10^{-6}\ \Omega^{-1}\ s^{n_\alpha}\ cm^{-2}$ with exponent $n_\alpha = 0.91$.

This approach was then extended to the impedance analysis at potentials close to $E_{1/2}$ by replacing the two capacitances $K_{ma}$ and $K_{ad}$ with two CPEs $Q_{ma}$ and $Q_{ad}$, respectively, in the equivalent circuit of Figure 2a. These two CPEs were assumed to share

the same exponent value $n_\alpha = 0.91$ so that their series combination $\left(Q_{ma}\left(j\omega\right)^{n_\alpha}\right)^{-1} + \left(Q_{ad}\left(j\omega\right)^{n_\alpha}\right)^{-1} = \left(Q_{md}\left(j\omega\right)^{n_\alpha}\right)^{-1}$ could be compared with the CPE value obtained at potentials far from $E_{1/2}$ [29]. Moreover, as stated previously, $C_d$ takes such high values that its contribution to the electrode impedance was neglected. On the basis of these considerations, the equivalent circuit in Figure 2a was replaced with its modified version in Figure 2b, where the diffuse layer capacity has been neglected and the monolayer capacities have been replaced by constant phase elements.

Figure 6 illustrates the influence of the electrode potential $E$ on the impedance Bode plots for two values of the surface concentration of ionizable groups. The $\Gamma_T^{p/dp}$ and $E_{1/2}$ values indicated in Figure 6, together with a value of $\omega_a = 0.986$, were derived from the integration and location, respectively, of low scan rate voltammetric peaks recorded under the same experimental conditions (a more detailed explanation can be found at the end of Section 2 in the Supporting Information). It may be observed how $-\Phi$ develops a progressively deeper minimum at $f^* \approx 10\ \mathrm{s}^{-1}$, as $E$ approaches $E_{1/2}$ from more anodic potentials. Simultaneously, the low-frequency $|Z_{cell}|$ values display an inflection point at frequencies close also to 10 $\mathrm{s}^{-1}$, and decrease as $E$ approaches $E_{1/2}$. The direction of these sequential variations of $-\Phi$ and $|Z_{cell}|$ is reversed when potentials are made progressively more negative than $E_{1/2}$ (not shown for clarity). The same behavior can be observed in the Bode plots reported by Burgess et al. [10] in their Figure 2. It may be noticed also in Figure 6 how $\Gamma_T^{p/dp}$ modulates the deviations of $-\Phi$ and $|Z_{cell}|$ with respect to the limiting $R_\Omega -$CPE behavior, in agreement with the theoretical predictions. In fact, the equivalent

circuit of Figure 2b reproduces satisfactorily the observed impedance spectrum, for any $\Gamma_T^{p/dp}$ and $E$ values, with fixed values of $R_\Omega = 280 \pm 30\ \Omega\ \mathrm{cm}^2$, $n_\alpha = 0.91$, $Q_{ma} = 90 \pm 20 \cdot 10^{-6}\ \Omega^{-1}\ \mathrm{s}^{0.91}\ \mathrm{cm}^{-2}$ and $Q_{ad} = 4.2 \pm 0.2 \cdot 10^{-6}\ \Omega^{-1}\ \mathrm{s}^{0.91}\ \mathrm{cm}^{-2}$, and the $C_{p/dp}$ and $R_{p/dp}$ values depicted in Figure 7.

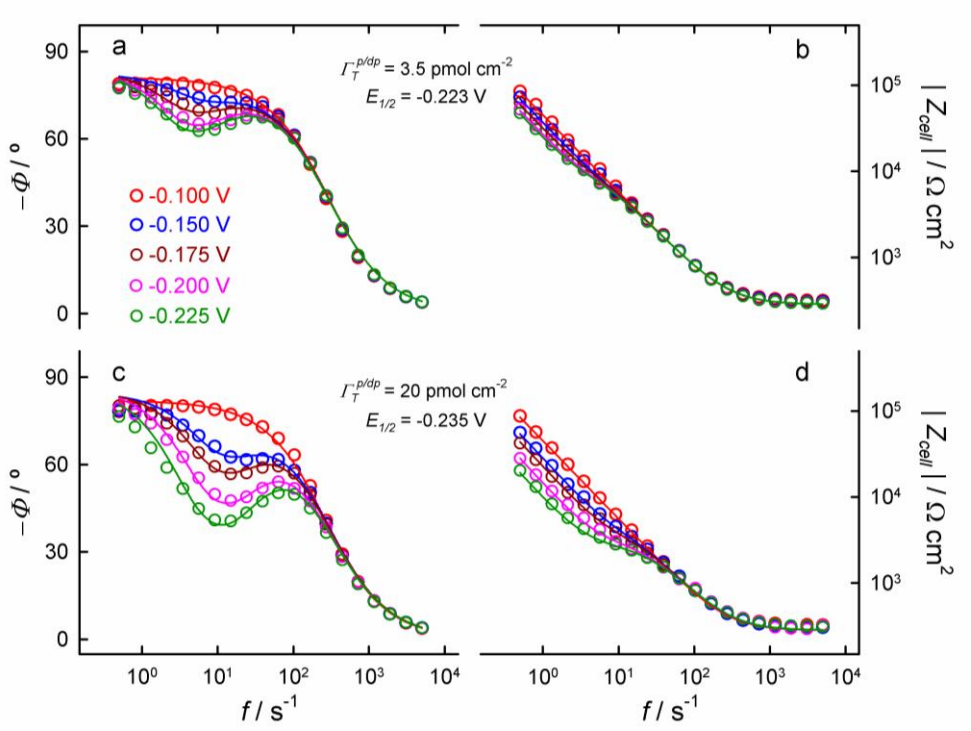


**Figure 6.** Influence of potential $E$ and surface concentration of carboxylic groups $\Gamma_T^{p/dp}$ on the Bode plots of a Au(111) electrode modified with a MUA monolayer, contacting a 20 mM NaF aqueous solution of pH 8.5 at 298 K. Values of $\Gamma_T^{p/dp}$, $E_{1/2}$ and $E$ are indicated in the Figure. Symbols are experimental data and lines are fits to the equivalent circuit in Figure 2b with $R_\Omega = 280 \pm 30\ \Omega\ \mathrm{cm}^2$, $n_\alpha = 0.91$, $Q_{ma} = 90 \pm 20 \cdot 10^{-6}\ \Omega^{-1}\ \mathrm{s}^{0.91}\ \mathrm{cm}^{-2}$, $Q_{ad} = 4.2 \pm 0.2 \cdot 10^{-6}\ \Omega^{-1}\ \mathrm{s}^{0.91}\ \mathrm{cm}^{-2}$, and the $C_{p/dp}$ and $R_{p/dp}$ values depicted in Figure 7.

Figure 7 illustrates the variation of $R_{p/dp}$ and $C_{p/dp}$ with the applied potential for four different values of $\Gamma_T^{p/dp}$. Besides a qualitative agreement with the theoretical trends illustrated in Figures 4c and 4d, satisfactory fits of these $R_{p/dp}$ and $C_{p/dp}$ values to eqs. 10 and 11 were obtained by using $\Gamma_T^{p/dp}$, $E_{1/2}$ and $\omega_a$ values derived independently from low scan rate voltammograms, as indicated before, and $k_s^{ap} = 9.4 \pm 0.5\ \mathrm{s}^{-1}$, $\alpha_p^{ap} = 0.45 \pm 0.03$ and $\alpha_M = 0.04 \pm 0.02$ (solid lines in Figure 6). Both $k_s^{ap}$ and $\alpha_p^{ap}$ values are in good agreement with those determined previously from the analysis of fast scan voltammograms recorded on the same system [11]. Since the $-\Phi$ values reported by Burgess et al. [10] develop a minimum at $f^* \approx 10\ \mathrm{s}^{-1}$, it can reasonably be assumed that their results are also consistent with $k_s^{ap} \approx 10\ \mathrm{s}^{-1}$.

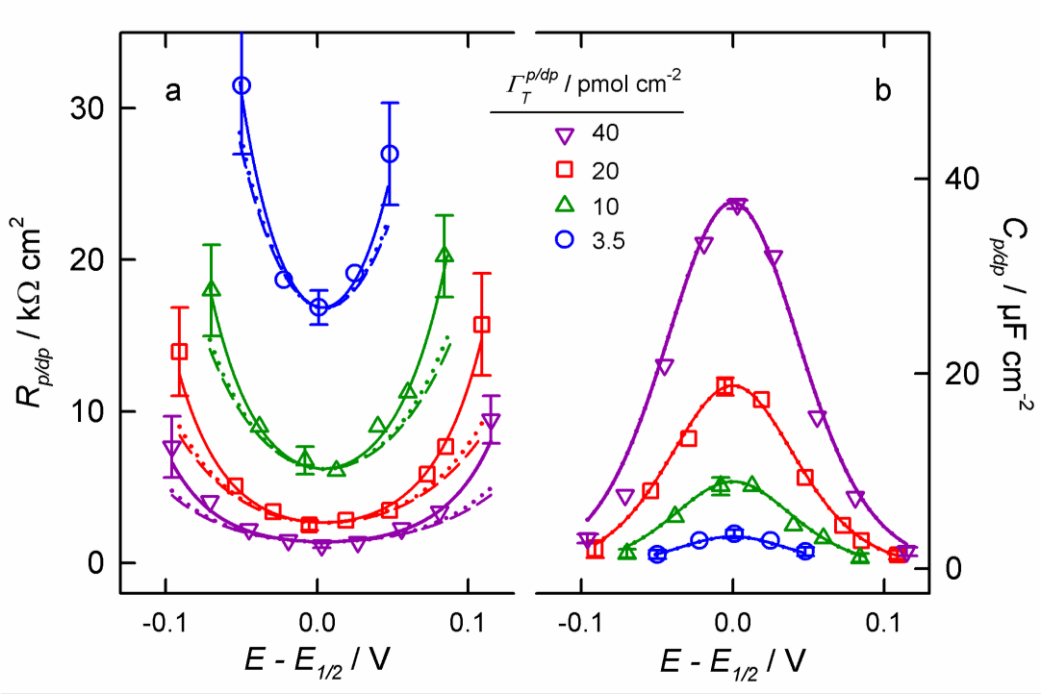

**Figure 7.** a) $R_{p/dp}$ and b) $C_{p/dp}$ values that fit the impedance spectrum of a Au(111) electrode modified with a MUA monolayer, contacting a 20 mM NaF aqueous solution of pH 8.5 at 298 K, as a function of overvoltage $E - E_{1/2}$ and surface concentration of carboxylic groups $\Gamma_T^{p/dp}$. Lines are theoretical values computed with eqs. 11 and 12 and the parameter values indicated in the text. Broken and dotted lines were computed by setting $\alpha_M = 0$ and 0.006, respectively.

---

Proton exchange between two adjacent oxygen atoms takes place typically in a time scale [30-32] much shorter than the 0.1 s determined for potential-induced proton transfer in MUA monolayers. Therefore, a mechanism based on a field-assisted displacement of the proton through the organic monolayer has been proposed before [11], in agreement with the observation that $\alpha_p^{ap} \approx \alpha_{dp}^{ap} \approx \omega_a / 2 = 0.49$, which implies that $\omega_b \approx 0$ (see eqs. S11 and S12), so that the proton acceptor and donor from solution remain close to the OHP, while their surface immobilized counterparts are close to the metal. On the other hand, the present estimate of $\alpha_M$ is significantly higher than the 0.006 value reported previously [11] (compare the dotted and full lines in Figure 7a). The new $\alpha_M$ value translates into a reorganization energy for proton transfer $\lambda$ (see eq. S13) of ~20 kJ mol$^{-1}$, much lower than our previous estimate of 80 kJ mol$^{-1}$. The present estimate of $\alpha_M$ is expected to be more accurate, since it has been obtained from experiments spanning a broader range of $\Gamma_T^{p/dp}$ values, but there may be a more fundamental reason that justifies the difference between the $\alpha_M$ values obtained from voltammetric and impedance measurements. In a recent study of the IR signature of MUA monolayers deposited on gold [19], we have observed a slow and reversible reorientation of the hydrocarbon chains upon application of a large potential

perturbation. Previously reported fast scan voltammetric experiments sampled a 1 V potential window in less than 50 ms, so that proton transfer took place at potentials far from $E_{1/2}$ in an effectively frozen monolayer structure. On the other hand, impedance measurements are collected at each potential after a 3 s delay to allow the monolayer to reorganize its molecular structure. Therefore, the variation in the proton transfer reorganization energy, as determined by voltammetric and impedance measurements, may just be a consequence of the slow response of the monolayer structure to changes in the applied potential.

## 5. Conclusions

The good agreement between the theoretically derived electrode impedance and the experimental results lends some additional support to our description of potential-induced proton transfers in acid thiol monolayers. This description is based upon two basic assumptions, a) proton transfer takes place according to a nonadiabatic mechanism and b) it involves a small population of physisorbed thiol molecules. The first assumption determines the potential dependence of the proton transfer parameters $R_{p/dp}$ and $C_{p/dp}$, which has been carefully examined over a ~200 mV potential window. The second assumption agrees with the consistent variation of $R_{p/dp}$ and $C_{p/dp}$ as the surface concentration of buried thiol molecules was systematically varied between 3.5 pmol cm$^{-2}$ and 40 pmol cm$^{-2}$. Voltammetric and impedance measurements provide the same values of the standard rate constant and transfer coefficients $\alpha_p^{ap} \approx \alpha_{dp}^{ap} \approx \omega_a / 2 = 0.49$ and, therefore, support the same physical picture of the proton transfer process. However, they produce different estimates of the reorganization energy that are tentatively ascribed to slow

changes in the molecular structure of the monolayer as the external potential is being varied. Derivation of explicit contributions to the cell impedance of potential-induced reorientation and dissociation of the external acid groups that would account for these types of effects, is currently underway.

**Acknowledgments**

This work was supported by the Spanish Ministry of Economy and Competitiveness and the European Union FEDER (grants CTQ2014-52641-P and CTQ2015-71955-REDT (ELECTROBIONET) ).

# Appendix A

# Supporting Information for:

# Proton Transfer Impedance of Electrodes Modified with Acid Thiol Monolayers

*Antonio M. Luque,*[a] *Willem H. Mulder,*[b] *Juan José Calvente* [a] *and Rafael Andreu* [a,*]

[a] Departamento de Química Física. Universidad de Sevilla. 41012-Sevilla, Spain

[b] Department of Chemistry, The University of the West Indies, Mona Campus, Kingston 7, Jamaica.

**1. Summary of thermodynamics and kinetics of the potential-induced proton transfer.**

This section is a summary of our previous work on the thermodynamics and kinetics of potential-induced proton transfer at self-assembled acid thiol monolayers [11,12]. In order to describe the electrochemical response of mercaptoalkanoic monolayers, we assume that the thiol monolayer contains two populations of carboxylic groups. The first one consists of those carboxylic groups that are exposed to the external solution, and whose ionization degree is determined only by their interaction with the solution components. The second one includes those carboxylic groups that are buried inside the monolayer, and whose ionization degree is controlled not only by the solution pH but also by the potential at the gold substrate $\phi^m$. We denote by $\Gamma_T^{ext}$ and $\Gamma_T^{p/dp}$ the surface concentrations of the external and buried carboxylic groups, respectively. The buried carboxylic (R-OH) and carboxylate ($R\text{-}O^-$) groups are assumed to be located at a plane *a* (see Figure S1), parallel to the electrode surface. The proton exchange process involves also a proton acceptor ($OH^-$) and a proton donor ($H_2O$) from solution, which share a common plane *b* of closest approach to the electrode surface (see Figure S1). Other electrolyte ions are allowed to approach the electrode up to plane *d* only, which can be identified with the Outer Helmholtz Plane. The average potential values at the first two planes, $\phi^a$ and $\phi^b$, with respect to the bulk solution ($\phi^s = 0$) can be expressed in terms of the electrode potential $\phi^m$, according to:

$$\phi^a = \phi^d + \omega_a \left( \phi^m - \phi^d - \frac{\theta_{R-O^-} F \Gamma_T^{p/dp}}{K_{ma}} \right) \qquad \text{(S1)}$$

where $\phi^d$ is the potential drop across the diffuse layer, $\theta_{R-O^-}$ is the ionization degree of the buried carboxylic groups, $\omega_a = K_{md} / K_{ad}$ is the ratio between the integral capacity of the

solvated monolayer ( $K_{md}$ ) and that of the dielectric slab limited by plane *a* and the diffuse layer boundary *d* ( $K_{ad}$ ), so that 0 < $\omega_a$ < 1, and $K_{ma}^{-1} = K_{md}^{-1} - K_{ad}^{-1}$.

Analogously,

$$\phi^b = \phi^d + \omega_b \left( \phi^m - \phi^d - \frac{\theta_{R-O^-} F \Gamma_T^{p/dp}}{K_{ma}} \right) \quad \text{(S2)}$$

where $\omega_b = K_{md} / K_{bd}$ .

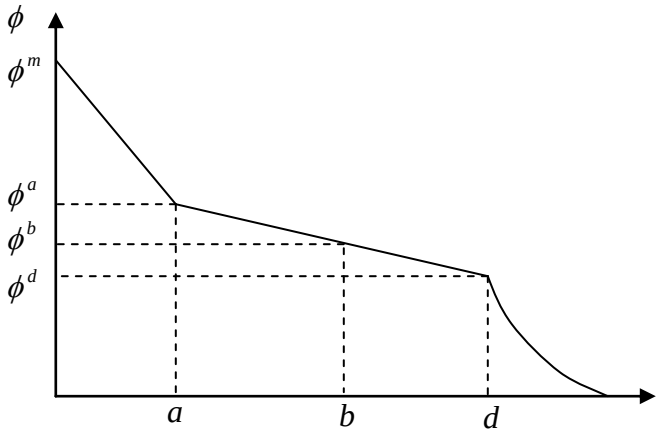


**Figure S1.** Schematic representation of the potential profile at the interface between a gold electrode modified with a $\omega$-mercaptoalkanoic acid monolayer and an aqueous electrolyte solution.

The equilibrium condition for proton transfer involving the buried carboxylic groups:

$$R-OH \text{ (plane a)} + OH^-(sol.) \rightleftharpoons R-O^- \text{ (plane a)} + H_2O \text{ (sol.)} \quad \text{(S3)}$$

can be expressed in terms of the electrochemical potentials of each species as:

$$\mu_{R-OH}^{0,a} + RT \ln \theta_{R-OH} + \mu_{OH^-}^{0,sol} + RT \ln a_{OH^-}^{sol} = \mu_{R-O^-}^{0,a} + RT \ln \theta_{R-O^-} - F\phi^a + \mu_{H_2O}^{0,sol} \quad \text{(S4)}$$

where $\theta_i = \Gamma_i^{p/dp} / \Gamma_T^{p/dp}$ and the other symbols have their usual meaning. This expression shows that $\theta_{R-O^-}$ depends on the applied electrode potential $\phi^m$ via eq S1. This relationship can be made explicit under equilibrium conditions, by combining eqs S1 and S4 to obtain:

$$\phi^m = \phi_{1/2}^m + \frac{\omega_a - 1}{\omega_a}(\phi^d - \phi_{1/2}^d) + \frac{RT}{\omega_a F}\ln\left(\frac{\theta_{R-O^-}}{1-\theta_{R-O^-}}\right) + \frac{(\theta_{R-O^-} - \frac{1}{2})F\Gamma_T^{p/dp}}{K_{ma}} \qquad \text{(S5)}$$

where $\phi_{1/2}^m$ is the half-conversion equilibrium potential, where $\theta_{R-O^-} = \theta_{R-OH}$, so that

$$\phi_{1/2}^m = \frac{\omega_a - 1}{\omega_a}\phi_{1/2}^d + \frac{\Delta G^0}{\omega_a F} - \frac{RT}{\omega_a F}\ln a_{OH^-}^{sol} + \frac{F\Gamma_T^{p/dp}}{2K_{ma}} \qquad \text{(S6)}$$

with $\Delta G^0 = \mu_{R-O^-}^{0,a} + \mu_{H_2O}^{0,sol} - \mu_{R-OH}^{0,a} - \mu_{OH^-}^{0,sol}$ and $\phi_{1/2}^d$ is the diffuse layer potential drop at $\phi_{1/2}^m$. Therefore, $\phi_{1/2}^m$ depends on the solution pH and the location and surface concentration of buried carboxylic groups.

Following our previous derivation [11], the net rate of deprotonation ($v$) can be expressed in terms of the deprotonation ($k_{dp}$) and protonation ($k_p$) rate constants as follows:

$$v = k_{dp} c_{OH^-}^{sol} \theta_{R-OH} - k_p \theta_{R-O^-} \qquad \text{(S7)}$$

where $k_p$ and $k_{dp}$ vary with $\phi^m$ according to:

$$\ln k_p = \ln k_s^{ap} - \alpha_p^{ap}\varphi - \alpha_M \varphi^2 \qquad \text{(S8)}$$

$$\ln\left(k_{dp} c_{OH^-}^{sol}\right) = \ln k_s^{ap} + \frac{F\left(\phi^d - \phi_{1/2}^d\right)}{RT} + \alpha_{dp}^{ap}\varphi - \alpha_M \varphi^2 \qquad \text{(S9)}$$

where $k_s^{ap}$ is the apparent standard rate constant of proton transfer and

$$\varphi = \frac{F}{RT}\left(\left(\phi^m - \phi_{1/2}^m\right) - \left(\phi^d - \phi_{1/2}^d\right) - \frac{\left(\theta_{R-O^-} - 1/2\right)F\Gamma_T^{p/dp}}{K_{ma}}\right) \qquad \text{(S10)}$$

$$\alpha_p^{ap} = \frac{\omega_a - \omega_b}{2}\left(1 - \frac{\Delta w_{1/2}}{\lambda}\right) \tag{S11}$$

$$\alpha_{dp}^{ap} = \frac{\omega_a + \omega_b}{2} + \frac{\omega_a - \omega_b}{2} \cdot \frac{\Delta w_{1/2}}{\lambda} \tag{S12}$$

$$\alpha_M = \frac{\left(\omega_a - \omega_b\right)^2 RT}{4\lambda} \tag{S13}$$

where $\lambda$ is the reorganization energy for the proton transfer step and $\Delta w_{1/2}$ is the difference between the amounts of work required to bring $H_2O$ and $OH^-$ from the solution to plane *b* when $\phi^m = \phi_{1/2}^m$. It is interesting to note that $\alpha_{dp}^{ap} + \alpha_p^{ap} = \omega_a$.

**2. Derivation of the proton transfer impedance.**

Let us consider a small periodic perturbation of the equilibrium film by a signal $\bar{\phi}^m + \Delta\phi^m e^{j\omega t}$, where the over-bar refers to the equilibrium state, $\omega$ is the perturbation angular frequency, $\Delta\phi^m$ the perturbation amplitude and $j = \sqrt{-1}$. The responses of $\theta_{R-O^-}$ and $\phi^d$ are represented as $\bar{\theta}_{R-O^-} + \Delta\theta_{R-O^-} e^{j\omega t}$ and $\bar{\phi}^d + \Delta\phi^d e^{j\omega t}$, respectively, where $\Delta\theta_{R-O^-}$ and $\Delta\phi^d$ are complex amplitudes that contain a frequency-dependent phase factor which accounts for the phase lag with respect to the applied signal. Now, the formula for the electrode admittance $Z_{el}^{-1}$ can be easily derived from eq. 4 in the main text, when the current density response is expressed as $\Delta i \cdot e^{j\omega t}$, to obtain:

$$Z_{el}^{-1}(j\omega) = \frac{\Delta i}{\Delta\phi^m} = j\omega\left(C_d \frac{\Delta\phi^d}{\Delta\phi^m} + F\Gamma_T^{p/dp} \frac{\Delta\theta_{R-O^-}}{\Delta\phi^m}\right) \tag{S14}$$

In order to determine the relationships between the $\Delta\theta_{R-O^-}$, $\Delta\phi^d$ and $\Delta\phi^m$ amplitudes, their previously formulated time dependence is substituted into eqs. 7 and 8 in

the main text. By retaining only terms up to first order in the various amplitudes, we get from eq. 7, after some rearrangement,

$$\left[ j\omega + \bar{k}_{dp} c_{OH^-}^{sol} + \bar{k}_p + \frac{\partial k_p}{\partial \theta_{R-O^-}} \bar{\theta}_{R-O^-} - \frac{\partial k_{dp}}{\partial \theta_{R-O^-}} c_{OH^-}^{sol} (1 - \bar{\theta}_{R-O^-}) \right] \Delta\theta_{R-O^-} +$$

$$+ \left[ \frac{\partial k_p}{\partial \phi^d} \bar{\theta}_{R-O^-} - \frac{\partial k_{dp}}{\partial \phi^d} c_{OH^-}^{sol} (1 - \bar{\theta}_{R-O^-}) \right] \Delta\phi^d = \left[ \frac{\partial k_{dp}}{\partial \phi^m} c_{OH^-}^{sol} (1 - \bar{\theta}_{R-O^-}) - \frac{\partial k_p}{\partial \phi^m} \bar{\theta}_{R-O^-} \right] \Delta\phi^m \quad \text{(S15)}$$

Analogously, we get from eq. 8,

$$\frac{F\Gamma_T^{p/dp}}{K_{ma}} \left[ -\bar{k}_{dp} c_{OH^-}^{sol} - \bar{k}_p + \frac{\partial k_{dp}}{\partial \theta_{R-O^-}} c_{OH^-}^{sol} (1 - \bar{\theta}_{R-O^-}) - \frac{\partial k_p}{\partial \theta_{R-O^-}} \bar{\theta}_{R-O^-} \right] \Delta\theta_{R-O^-} + ..$$

$$.. + \left[ j\omega \left( 1 + \frac{C_d}{K_{md}} \right) + \frac{F\Gamma_T^{p/dp}}{K_{ma}} \left( \frac{\partial k_{dp}}{\partial \phi^d} c_{OH^-}^{sol} (1 - \bar{\theta}_{R-O^-}) - \frac{\partial k_p}{\partial \phi^d} \bar{\theta}_{R-O^-} \right) \right] \Delta\phi^d = ..$$

$$.. = \left[ j\omega + \frac{F\Gamma_T^{p/dp}}{K_{ma}} \left( \frac{\partial k_p}{\partial \phi^m} \bar{\theta}_{R-O^-} - \frac{\partial k_{dp}}{\partial \phi^m} c_{OH^-}^{sol} (1 - \bar{\theta}_{R-O^-}) \right) \right] \Delta\phi^m \quad \text{(S16)}$$

Eqs. S15 and S16 are two simultaneous linear equations in terms of the complex amplitudes $\Delta\theta_{R-O^-}$ and $\Delta\phi^d$, that can be rewritten in a more manageable form as:

$$(j\omega + \alpha_{11}) \Delta\theta_{R-O^-} + \alpha_{12} \Delta\phi^d = \beta_1 \Delta\phi^m \quad \text{(S17)}$$

and

$$\alpha_{21} \Delta\theta_{R-O^-} + (j\omega\zeta + \alpha_{22}) \Delta\phi^d = (j\omega + \beta_2) \Delta\phi^m \quad \text{(S18)}$$

where some coefficients are related by: $\alpha_{21} = -F\Gamma_T^{p/dp} \alpha_{11} / K_{ma}$, $\alpha_{22} = -F\Gamma_T^{p/dp} \alpha_{12} / K_{ma}$ and $\beta_2 = -F\Gamma_T^{p/dp} \beta_1 / K_{ma}$.

By solving eqs. S17 and S18, and substituting for $\Delta\theta_{R-O^-}$ and $\Delta\phi^d$ into eq. S14, we obtain for the frequency dispersion of the electrode admittance:

$$Z_{el}^{-1}(j\omega) = j\omega \frac{-C_d\omega^2 + j\omega\left[C_d\left(\alpha_{11} - \frac{F\Gamma_T^{p/dp}}{K_{ma}}\beta_1\right) + F\Gamma_T^{p/dp}(\zeta\beta_1 - \alpha_{12})\right]}{-\zeta\omega^2 + j\omega\left(\zeta\alpha_{11} - \frac{F\Gamma_T^{p/dp}}{K_{ma}}\alpha_{12}\right)} \tag{S19}$$

This frequency dependence is identical to that of the equivalent circuit depicted in Figure S2a, for which:

$$Z_{circuit}^{-1}(j\omega) = j\omega C_1 \frac{-RC_2C_3\omega^2 + j\omega(C_2 + C_3)}{-RC_3(C_1 + C_2)\omega^2 + j\omega(C_1 + C_2 + C_3)} \tag{S20}$$

It should be noted that the interpretation of the four circuit elements is not unique, since identifying the two expressions results in only three independent equations in terms of the four unknowns $C_1, C_2, C_3$ and $R$. However, from the physical model, it is clear that we should identify $C_1$ with $K_{ma}$. The remaining circuit elements then follow from comparison of ratios of the corresponding coefficients in the two admittance formulae. After some algebra we find the following relationships between circuit elements and model parameters:

$$\frac{1}{C_2} = \frac{1}{C_{as}} = \frac{1}{K_{ad}} + \frac{1}{C_d} \tag{S21}$$

$$R = R_{p/dp} = \left[F\Gamma_T^{p/dp}\left(1 + \frac{K_{ad}C_d}{K_{ma}(K_{ad} + C_d)}\right)\left(\beta_1 - \frac{\alpha_{12}}{1 + C_d / K_{md}}\right)\right]^{-1} \tag{S22}$$

$$C_3 = C_{p/dp} = \left(K_{ma} + \frac{K_{ad}C_d}{K_{ad} + C_d}\right)\frac{1 - \frac{\alpha_{12}}{\beta_1(1 + C_d / K_{md})}}{\frac{\alpha_{11}K_{ma}}{F\Gamma_T^{p/dp}\beta_1} - 1} \tag{S23}$$

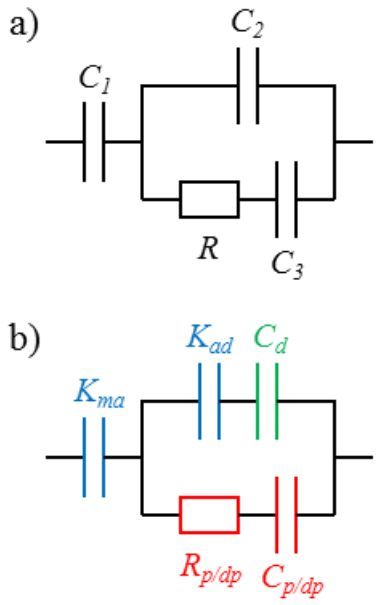


**Figure S2.** a) Combination of three capacitors $C_1$, $C_2$ and $C_3$ and a resistor $R$ that reproduces the frequency dependence of the modified electrode admittance, as derived from the present model. b) Identification of the equivalent circuit elements in terms of the model parameters. The subscript *p/dp* refers to the protonation / deprotonation process.

In order to express the components of the equivalent circuit more explicitly in terms of the actual model parameters, we need to evaluate $\alpha_{11}$, $\alpha_{12}$ and $\beta_1$ using their respective definitions and the formulae for $k_p$ and $k_{dp}c_{OH^-}^{sol}$, keeping in mind the fact that in equilibrium $\bar{k}_{dp}c_{OH^-}^{sol}(1-\bar{\theta}_{R-O^-}) = \bar{k}_p\bar{\theta}_{R-O^-}$. A straightforward calculation leads to the following, remarkably simple, results: $\beta_1 = \frac{\omega_a F}{RT}\bar{k}_p\bar{\theta}_{R-O^-}$, $\alpha_{12} = \frac{\omega_a - 1}{\omega_a}\beta_1$ and

$\alpha_{11} = \bar{k}_{dp} c_{OH^-}^{sol} + \bar{k}_p + \frac{F\Gamma_T^{p/dp}}{K_{ma}} \beta_1$, which, when inserted into the expressions for $C_{p/dp}$ and $R_{p/dp}$, yield the desired formulae

$$C_{p/dp} = \frac{F^2 \Gamma_T^{p/dp}}{RT} \bar{\theta}_{R-O^-} \left(1 - \bar{\theta}_{R-O^-}\right) = \frac{F^2 \Gamma_T^{p/dp}}{RT} \frac{\exp\left(\frac{F\left(\phi^d - \phi_{1/2}^d\right)}{RT} + \omega_a \varphi\right)}{\left(1 + \exp\left(\frac{F\left(\phi^d - \phi_{1/2}^d\right)}{RT} + \omega_a \varphi\right)\right)^2} \quad \text{(S24)}$$

$$R_{p/dp} = \frac{RT}{F^2 \Gamma_T^{p/dp}} \frac{1}{\bar{k}_p \bar{\theta}_{R-O^-}} = \frac{RT}{F^2 \Gamma_T^{p/dp}} \left(\frac{1}{\bar{k}_p} + \frac{1}{\bar{k}_{dp} c_{OH^-}^{sol}}\right) \quad \text{(S25)}$$

We have shown previously [11,12] that $\phi^d$ remains invariant within the potential window of interest when $\Gamma_{R-O^-}^{ext} \geq 100$ pmol cm$^{-2}$, which applies under our working conditions. Then, $\phi^d - \phi_{1/2}^d = 0$, $\phi^m - \phi_{1/2}^m = E - E_{1/2}$ and eq. S10 simplifies to:

$$\varphi = \frac{F}{RT}\left(E - E_{1/2} - \frac{\left(\bar{\theta}_{R-O^-} - 1/2\right) F \Gamma_T^{p/dp}}{K_{ma}}\right) \quad \text{(S26)}$$

In order to compare theoretical predictions from the above equations with experimental results, the values of $E_{1/2}$, $\omega_a$ and $\Gamma_T^{p/dp}$ can be obtained from the location and shape of low scan rate voltammograms recorded under the same experimental conditions [12]. $E_{1/2}$ coincides with the voltammetric peak potential, the area under the voltammetric peak is equal to the product $\omega_a F \nu \cdot \Gamma_T^{p/dp}$ and the full width at half height of the peak is given by $\left(3.52RT / \omega_a F\right) + \left(1.075 \cdot \left(1 - \omega_a\right) \cdot \nu F \Gamma_T^{p/dp} / K_{md}\right)$. Finally, the fraction of ionized groups $\bar{\theta}_{R-O^-}$ at a given potential $E$ can be obtained by solving the equilibrium condition:

$$E = E_{1/2} + \frac{RT}{\omega_a F}\left[\ln\left(\frac{\bar{\theta}_{R-O^-}}{1-\bar{\theta}_{R-O^-}}\right) + \frac{(1-\omega_a)\cdot\omega_a F^2 \Gamma_T^{P/dp}\bar{\theta}_{R-O^-}}{K_{md}RT}\right] \quad \text{(S27)}$$

where typically $K_{md} \approx 2.5\ \mu\text{F cm}^{-2}$ for MUA monolayers.

**3. Influence of the kinetic parameters on the proton transfer resistance.**

Figure S3 illustrates the influence of the kinetic parameters $k_s^{ap}$, $\alpha_p^{ap}$ and $\alpha_M$ on the variation of $R_{p/dp}$ with the applied potential. It may be observed that the $R_{p/dp}$ values are proportional to $1/k_s^{ap}$ at any potential (Figure S3a), whereas the slopes of these $R_{p/dp}$ vs. $E$ plots are mainly determined by the values of $\alpha_p^{ap}$, $\alpha_{dp}^{ap}$ and $\alpha_M$. Whenever $\alpha_{dp}^{ap} > \alpha_p^{ap}$ ($\alpha_{dp}^{ap} < \alpha_p^{ap}$), a higher slope is predicted for the cathodic (anodic) branch of the $R_{p/dp}$ vs. $E$ curve, since $k_{dp}$ ($k_p$) then varies faster than $k_p$ ($k_{dp}$) with the applied potential (Figure S3b). This lack of symmetry in the potential dependence of the two rate constants produces also a displacement of the potential $E_{min}$ at which the minimum value of $R_{p/dp}$ is observed, which in the case of $\alpha_M = 0$ and $\Gamma_T^{p/dp} \to 0$ is given by:

$$E_{min} = E_{1/2} + \frac{RT}{\omega_a F}\ln\frac{\alpha_{dp}^{ap}}{\alpha_p^{ap}} \quad \text{(S28)}$$

On the other hand, the influence of $\alpha_M$ is more evident at potentials far from $E_{1/2}$, where it produces a symmetric broadening of the $R_{p/dp}$ vs. $E$ curve, since it exerts the same inhibiting effect on $k_p$ and $k_{dp}$ at a given $|E - E_{1/2}|$.

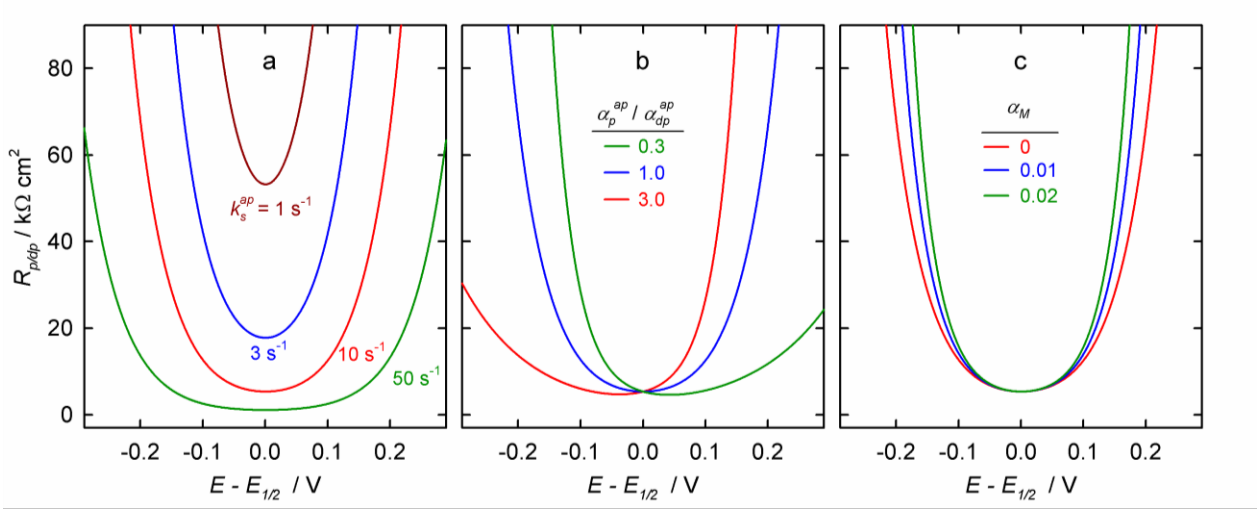


**Figure S3.** Influence of a) $k_s^{ap}$, b) the $\alpha_p^{ap} / \alpha_{dp}^{ap}$ ratio and c) $\alpha_M$ on the variation of $R_{p/dp}$ with the applied potential. Default parameter values: $\Gamma_T^{p/dp} = 10$ pmol cm$^{-2}$, $k_s^{ap} = 10$ s$^{-1}$, $\omega_a = 0.9$, $\alpha_p^{ap} = \omega_a / 2$, $\alpha_M = 0$, $K_{md} = 3\ \mu$F cm$^{-2}$, $\Gamma_{R-O^-}^{ext} = 400$ pmol cm$^{-2}$, $T = 298$ K.

**References**

[1] R. Parsons, General equations for the kinetics of electrode processes, Trans. Faraday Soc. 47 (1951) 1332-1344.

[2] W. R. Fawcett, Potential dependence of the elementary steps in the kinetics of electrode reactions involving amalgam formation, J. Phys. Chem. 93 (1989) 2675-2682.

[3] C. Ma, J. M. Harris, Surface-enhanced Raman spectroscopy investigation of the potential-dependent acid-base chemistry of silver-immobilized 2-mercaptobenzoic acid, Langmuir 27 (2011) 3527-3533.

[4] R. Martínez-Hincapié, A. Berná, A. Rodes, V. Climent, J. M. Feliu, Surface acid-base properties of anion-adsorbed species at Pt(111) electrode surfaces in contact with $CO_2$-containing perchloric acid solutions, J. Phys. Chem. C 120 (2016) 16191-16199.

[5] S. Gan, L. Zhong, L. Gao, D. Han, L. Niu, Electrochemically driven surface-confined acid/base reaction for an ultrafast $H^+$ supercapacitor, J. Am. Chem. Soc. C 138 (2016) 1490-1493.

[6] J. C. Love, L. A. Estroff, J. K. Kriebel, R. G. Nuzzo, G. M. Whitesides, Self-assembled monolayers of thiolates on metals as a form of Nanotechnology, Chem. Rev. 105 (2005) 1103-1170.

[7] C. Vericat, M. E. Vela, G. Benitez, P. Carro, R. C. Salvarezza, Self-assembled monolayers of thiols and dithiols on gold: new challenges for a well-known system, Chem. Soc. Rev. 39 (2010) 1805-1834.

[8] J. J. Gooding, S. Ciampi, The molecular level modification of surfaces: from self-assembled monolayers to complex molecular assemblies, Chem. Soc. Rev. 40 (2011) 2704-2718.

[9] H. S. White, J. D. Peterson, Q. Cui, K. J. Stevenson, Voltammetric measurement of interfacial acid/base reactions, J. Phys. Chem. B 102 (1998) 2930-2934.

[10] I. Burgess, B. Seivewright, R. B. Lennox, Electric field driven protonation/deprotonation of self-assembled monolayers of acid-terminated thiols, Langmuir 22 (2006) 4420-4428.

[11] A. M. Luque, W. H. Mulder, J. J. Calvente, A. Cuesta, R. Andreu, Proton transfer voltammetry at electrodes modified with acid thiol monolayers, Anal. Chem. 84 (2012) 5778-5786.

[12] J. J. Calvente, A. M. Luque, R. Andreu, W. H. Mulder, J. L. Olloqui-Sariego, Analytical expressions for proton transfer voltammetry: analogy to surface redox voltammetry with Frumkin interactions, Anal. Chem. 85 (2013) 4475-4482.

[13] S. M. Rosendahl, I. J. Burgess, Electrochemical and infrared spectroscopy studies of 4-mercaptobenzoic acid SAMs on gold surfaces, Electrochim. Acta 53 (2008) 6759-6767.

[14] Y. Chen, X. Yang, B. Jin, L. Guo, L. Zheng, X. Xia, Preparation and interfacial properties of phosphonic acid-terminated self-assembled monolayers on gold surface, J. Phys. Chem. C 113 (2009) 4515-4521.

[15] J. Pillay, B. O. Agboola, K. I. Ozoemena, Electrochemistry of 2-dimethylaminoethanothiol SAM on gold electrode: Interaction with SWCNT-poly(*m*-

aminobenzene sulphonic acid), electric field-induced protonation-deprotonation, and surface $pK_a$, Electrochem. Comm. 11 (2009) 1292-1296.

[16] K. Sugihara, K. Shimazu, K. Uosaki, Electrode potential effect on the surface $pK_a$ of a self-assembled 15-mercaptohexadecanoic acid monolayer on a gold/quartz crystal microbalance electrode, Langmuir 16 (2000) 7101-7105.

[17] N. Goutev, M. Futamata, Attenuated total reflection surface-enhanced infrared absorption spectroscopy of carboxyl terminated self-assembled monolayers on gold, Appl. Spectrosc. 57 (2003) 506-513.

[18] M. Futamata, Characterization of the first layer and second layer adsorbates on Au electrodes using ATR-IR spectroscopy, J. Electroanal. Chem. 550-551 (2003) 93-103.

[19] A. M. Luque, A. Cuesta, J. J. Calvente, R. Andreu, Potentiostatic infrared titration of 11-mercaptoundecanoic acid monolayers, Electrochem. Commun. 45 (2014) 13-16.

[20] E. Laviron, Voltammetric methods for the study of adsorbed species, vol. 12 in Electroanalytical Chemistry. Edited by A. J. Bard. New York: Marcel Dekker; 1982: 53-157.

[21] M. Sluyters-Rehbach, J. H. Sluyters, The a.c. techniques [for studying electrodics], vol. 9 in Comprehensive Treatise of Electrochemistry. Edited by E. Yeager. New York: Plenum Press; 1984: 177-292.

[22] E. Laviron, A.c. polarography and faradaic impedance of strongly adsorbed electroactive species. Part III. Theoretical complex plane analysis for a surface redox reaction, J. Electroanal. Chem. 105 (1979) 35-42.

[23] M. Rueda Rueda, F. Prieto Dapena, Application of electrochemical impedance spectroscopy to the study of surface processes, Collect. Czech. Chem. Commun. 76 (2011) 1825-1854.

[24] P. R. Bueno, F. Fabregat-Santiago, J. J. Davis, Elucidating capacitance and resistance terms in confined electroactive molecular layers, Anal. Chem. 85 (2013) 411-417.

[25] E. Boubour, R. B. Lennox, Stability of ω-functionalized self-assembled monolayers as a function of applied potential, Langmuir 16 (2000) 7464-7470.

[26] T. Pajkossy, Impedance spectroscopy at interfaces of metals and aqueous solutions – Surface roughness, CPE and related issues, Solid State Ion. 176 (2005) 1997-2003.

[27] A. S. Bandarenka, Exploring the interfaces between metal electrodes and aqueous electrolytes with electrochemical impedance spectroscopy, Analyst 138 (2013) 5540-5554.

[28] T. Pajkossy, R. Jurczakowski, Electrochemical impedance spectroscopy in interfacial studies, Curr. Opin. Electrochem. 1 (2017) 53-58.

[29] M. Kokoschka, J. B. Henry, A. S. Bandarenka, Multiparametric characterization of nonelectroactive self-assembled monolayers during their formation, Langmuir 29 (2013) 9909-9917.

[30] M. L. Donten, J. VandeVondele, P. Hamm, Speed limits for acid-base chemistry in aqueous solutions, Chimia 66 (2012) 182-186.

[31] U. Rivard, V. Thomas, A. Bruhacs, B. Siwick, R. Iftimie, Donor-bridge-acceptor proton transfer in aqueous solution, J. Phys. Chem. Lett. 5 (2014) 3200-3205.

[32] N. Agmon, H. J. Bakker, R. K. Campen, R. H. Henchman, P. Pohl, S. Roke, M. Thämer, A. Hassanali, Protons and hydroxide ions in aqueous systems, Chem. Rev. 116 (2016) 7642-7672.

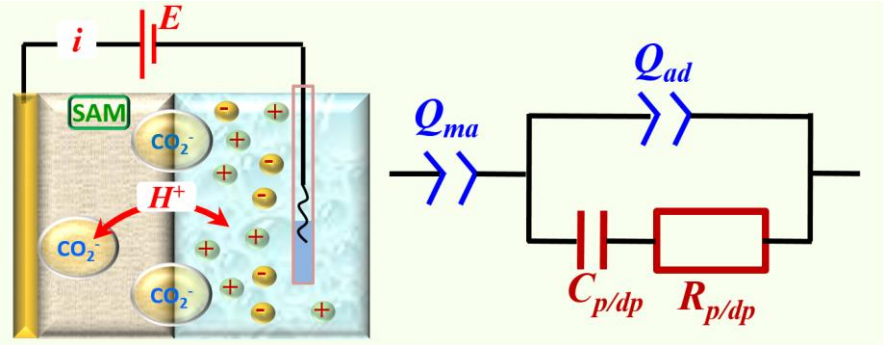


**TOC Graphic**